

Supporting Information for

Bulk Photovoltaic Effect in GaNGeC Quaternary Compound

Semiconductors

Ping Lou^{*,†,‡} and Jin Yong Lee^{*,†}

*Department of Chemistry, Sungkyunkwan University, Suwon 16419, Korea, and Department of
Physics, Anhui University, Hefei 230039, Anhui, China*

E-mail: loup@ahu.edu.cn; jinylee@skku.edu

*To whom correspondence should be addressed

†Department of Chemistry, Sungkyunkwan University, Suwon 16419, Korea

‡Department of Physics, Anhui University, Hefei 230039, Anhui, China

Table of Contents

1. Table S1: Fractional Coordinates of the Atom in the Primitive Cell — S3
2. Figure S1: Shift current conductivity tensor spectra of S-1 crystal — S4
3. Figure S2: Shift current conductivity tensor spectra of S-2 crystal — S4
4. Figure S3: Shift current conductivity tensor spectra of S-3 crystal — S5
5. Figure S4: Shift current conductivity tensor spectra of S-4 crystal — S5
6. Figure S5: Shift current conductivity tensor spectra of S-5 crystal — S6
7. Figure S6: Shift current conductivity tensor spectra of S-6 crystal — S6
8. Figure S7: S-1, S-5 and S-6 crystals — S7
9. Figure S8: Shift current tensor spectra of GaN crystal — S8
10. Figure S9: Charge density, ELF, and DCD for GaN — S8
11. Figure S10: Charge density, ELF, and DCD for S-1 — S9
12. Figure S11: Charge density, ELF, and DCD for S-5 — S9
13. Figure S12: Charge density, ELF, and DCD for S-6 — S10
14. Figure S13: PBE and GW shift current conductivity tensors of S-1 crystal — S11
15. Figure S14: PBE and GW shift current conductivity tensors of S-2 crystal — S11
16. Figure S15: PBE and GW shift current conductivity tensors of S-3 crystal — S12
17. Figure S16: PBE and GW shift current conductivity tensors of S-4 crystal — S12
18. Figure S17: PBE and GW shift current conductivity tensors of S-5 crystal — S13
19. Figure S18: PBE and GW shift current conductivity tensors of S-6 crystal — S13
20. Figure S19: PBE and GW shift current conductivity tensors of GaN crystal — S14
21. Figure S20, Quantum molecular dynamics simulations for S-1 crystal stacking — S15
22. Figure S21, Quantum molecular dynamics simulations for S-2 crystal stacking — S16
23. Figure S22, Quantum molecular dynamics simulations for S-3 crystal stacking — S17
24. Figure S23, Quantum molecular dynamics simulations for S-4 crystal stacking — S18
25. Figure S24, Quantum molecular dynamics simulations for S-5 crystal stacking — S19
26. Figure S25, Quantum molecular dynamics simulations for S-6 crystal stacking — S20
27. Figure S26, *Ab initio* and Wannier-interpolated bands of s-1, -2, -3, -4, -5, and -6 — S21
28. Discussion S1, Influence of Spatial Symmetry on the Linear Optical Conductivity — S22
29. Discussion S2, Influence of Spatial Symmetry on the Shift Current Conductivity — S23

Table S1: Fractional Coordinates of the Atoms in the Primitive Cell, and Wyckoff Positions of Group.

	S-1	<i>P3m1</i> (No.156)
Ge	0.66666666666666714, 0.3333333333333286, 0.3624599819999971	1c
C	0.3333333333333286, 0.66666666666666714, 0.4790199799999968	1b
Ga	0.3333333333333286, 0.66666666666666714, 0.8624199910000031	1b
N	0.66666666666666714, 0.3333333333333286, 0.9960899690000034	1c
	S-2	<i>Pmm2</i> (No. 25)
Ge	0.5000000000000000, 0.0000000000000000, 0.3069426505183119	1c
C	0.0000000000000000, 0.0000000000000000, 0.5409335387865466	1a
Ga	0.0000000000000000, 0.5000000000000000, 0.7934918935126746	1b
N	0.5000000000000000, 0.5000000000000000, 0.0586318951824683	1d
	S-3	<i>Pmm2</i> (No. 25)
Ge	0.0000000000000000, 0.0000000000000000, 0.5877554933025234	1a
C	0.5000000000000000, 0.0000000000000000, 0.8216899701073591	1c
Ga	0.5000000000000000, 0.5000000000000000, 0.0742271464295536	1d
N	0.0000000000000000, 0.5000000000000000, 0.3394273351605525	1a
	S-4	<i>Pmm2</i> (No. 25)
Ge	0.5000000000000000, 0.5000000000000000, 0.8158552834755285	1d
C	0.0000000000000000, 0.5000000000000000, 0.5818794706489309	1b
Ga	0.0000000000000000, 0.0000000000000000, 0.3293138608568018	1a
N	0.5000000000000000, 0.0000000000000000, 0.0641713230187433	1c
	S-5	<i>R3m</i> (No. 160)
Ge	0.6709841743474934, 0.6709841743474934, 0.6709841743474934	1a
C	0.2911739297909084, 0.2911739297909084, 0.2911739297909084	1a
Ga	0.8190742803260118, 0.8190742803260118, 0.8190742803260118	1a
N	0.1995873262022444, 0.1995873262022444, 0.1995873262022444	1a
	S-6	<i>P3m1</i> (No.156)
Ge	0.6666667436180234, 0.3333333243819752, 0.3305940463622838	1c
C	0.3333333069338735, 0.6666667660661290, 0.1905461627035190	1b
Ga	0.6666668219594882, 0.3333332460405103, 0.7739294995641177	1c
N	0.3333332694886195, 0.6666668035113830, 0.9157003673700826	1b

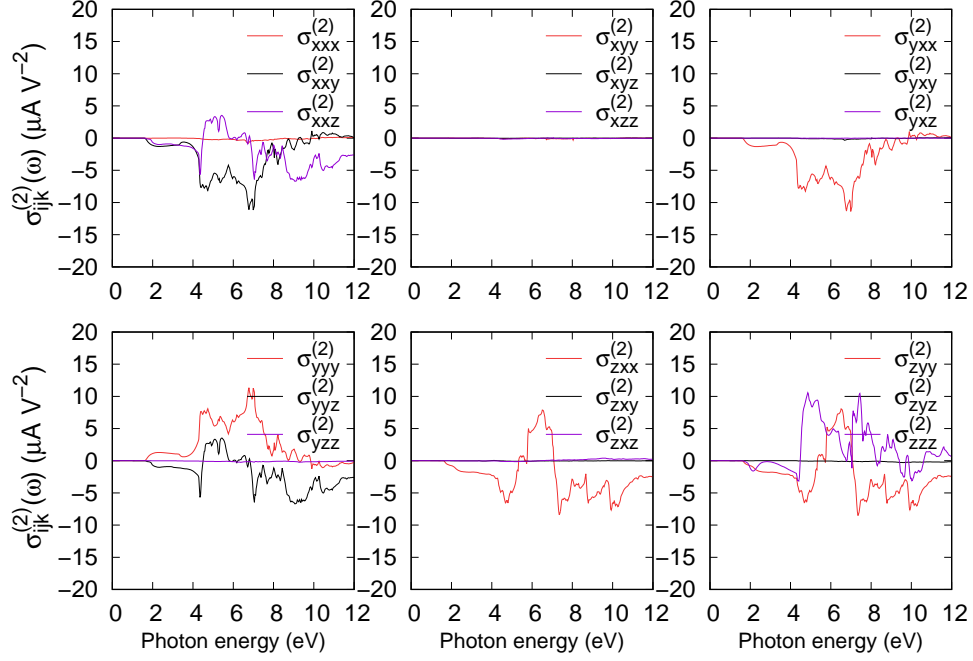


Figure S1: (Color online) Shift current conductivity tensor $\sigma_{ijk}^{(2)}(\omega)$ spectra of S-1 crystal, where ω is the photon energy, and $i, j, k = x, y, z$.

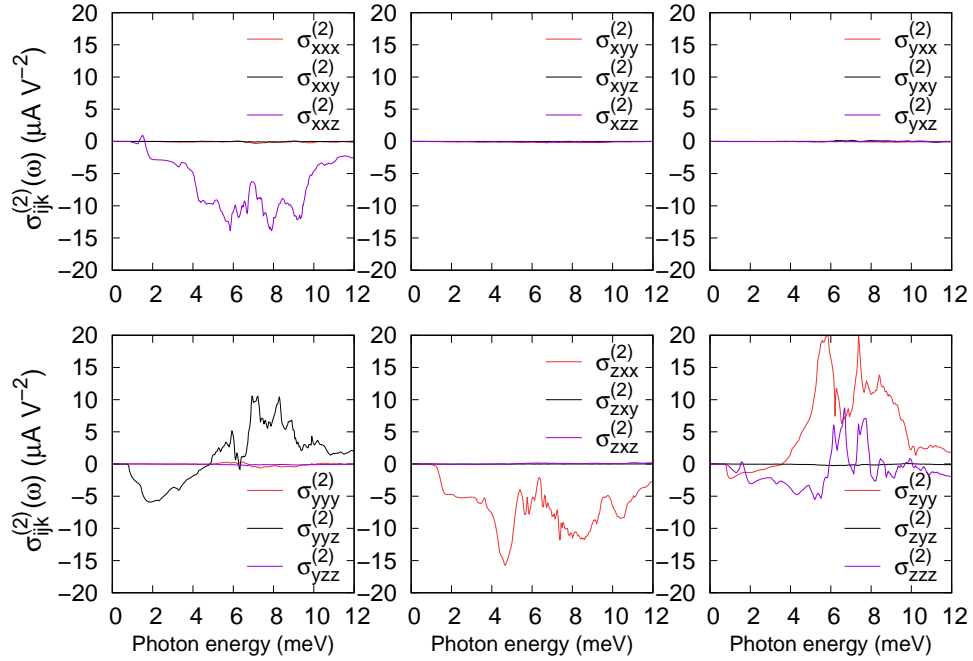


Figure S2: (Color online) Shift shift current conductivity tensor $\sigma_{ijk}^{(2)}(\omega)$ spectra of S-2 crystal, where ω is the photon energy, and $i, j, k = x, y, z$.

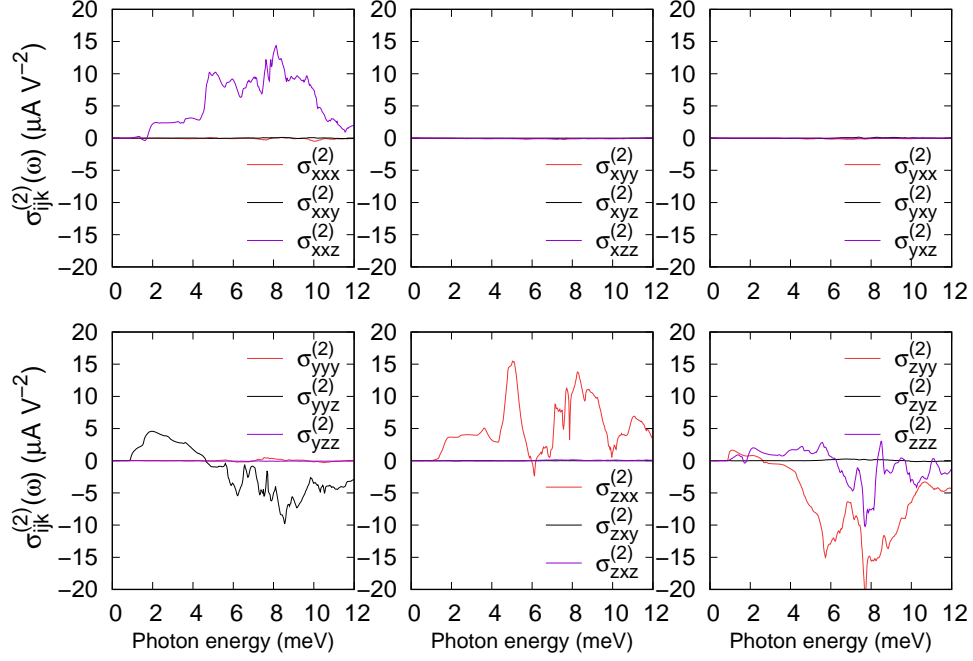


Figure S3: (Color online) Shift current conductivity tensor $\sigma_{ijk}^{(2)}(\omega)$ spectra of S-3 crystal, where ω is the photon energy, and $i, j, k = x, y, z$.

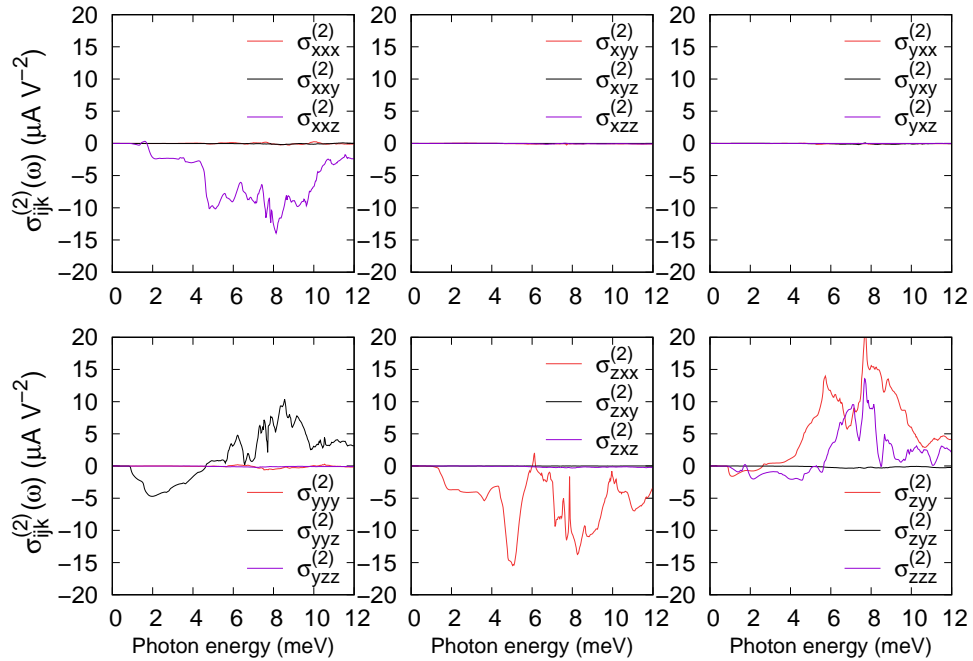


Figure S4: (Color online) Shift current conductivity tensor $\sigma_{ijk}^{(2)}(\omega)$ spectra of S-4 crystal, where ω is the photon energy, and $i, j, k = x, y, z$.

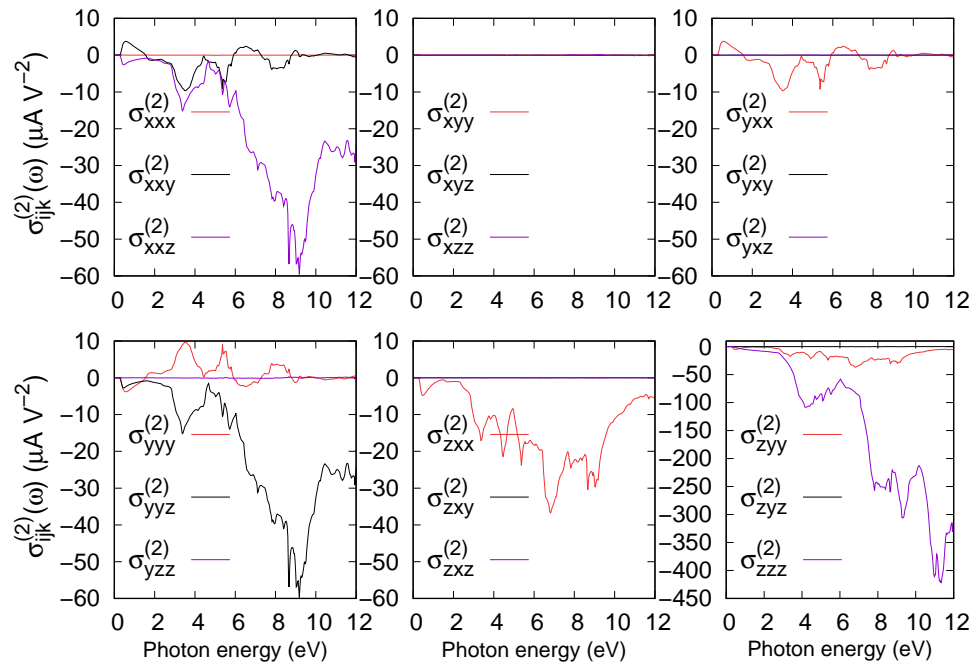


Figure S5: (Color online) Shift current conductivity tensor $\sigma_{ijk}^{(2)}(\omega)$ spectra of S-5 crystal, where ω is the photon energy, and $i, j, k = x, y, z$.

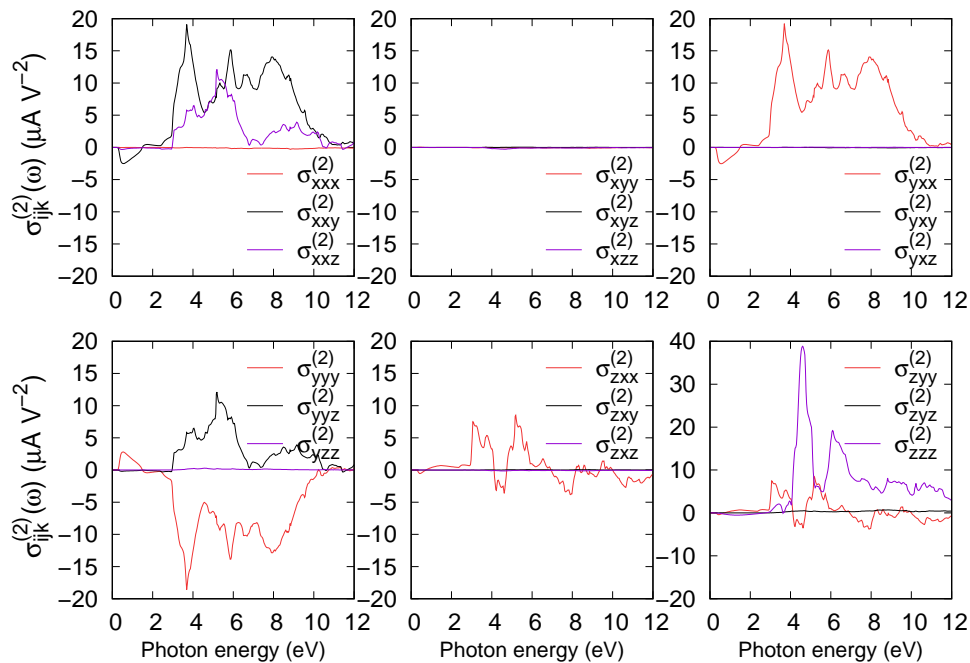


Figure S6: (Color online) Shift current conductivity tensor $\sigma_{ijk}^{(2)}(\omega)$ spectra of S-6 crystal, where ω is the photon energy, and $i, j, k = x, y, z$.

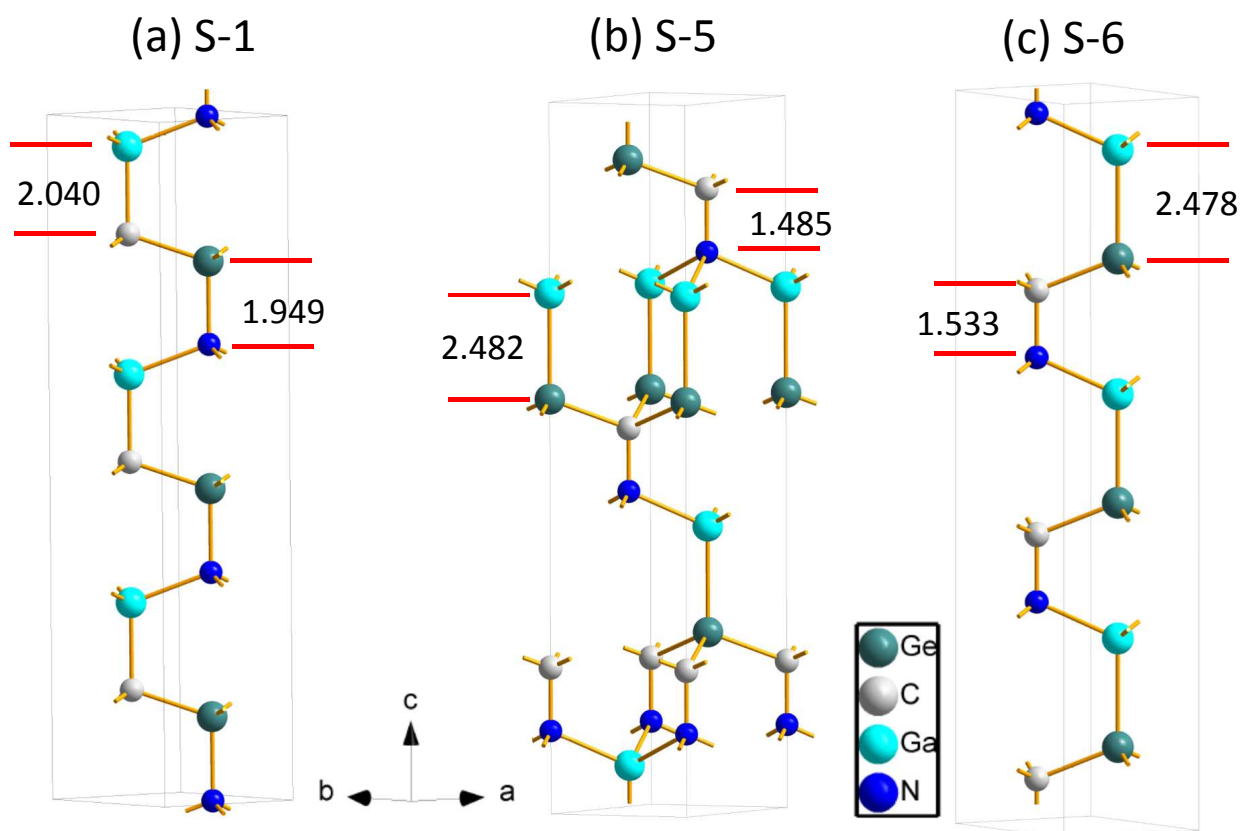


Figure S7: (Color online) (a) S-1 $1 \times 1 \times 3$ supercell, (b) S-5 hexagonal unit cell, and (c) S-6 $1 \times 1 \times 3$ super unit cells. The numbers 2.040 and 1.949 in (a) indicate the bonding length of C-Ga and the bonding length of N-Ge, and the unit is Å. The numbers 2.482 and 1.485 in (b) indicate the bonding length of Ge-Ga and the bonding length of N-C, and the unit is Å. The numbers 2.478 and 1.533 in (c) indicate the bonding length of Ge-Ga and the bonding length of C-N, and the unit is Å.

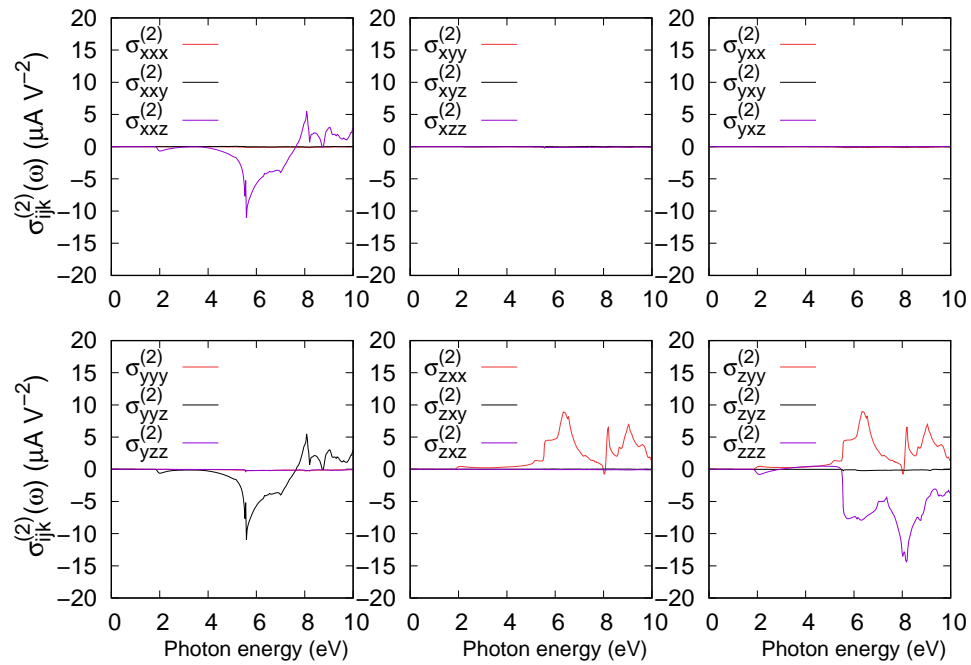


Figure S8: (Color online) Shift current tensor $\sigma_{ijk}^{(2)}(\omega)$ spectra of GaN crystal, where ω is the photon energy, and $i, j, k = x, y, z$.

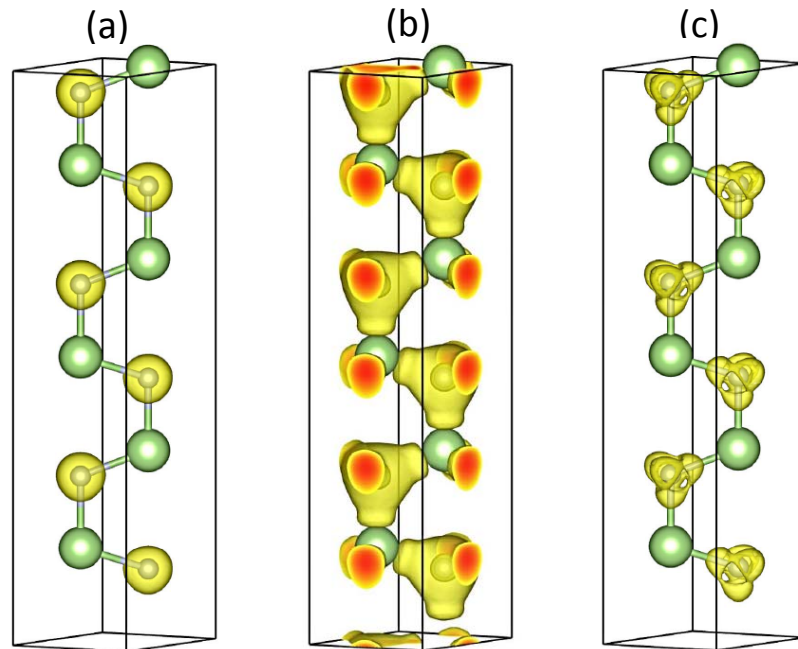


Figure S9: (Color online) (a) Charge density at isosurface level 0.17, (b) Electron localization function at isosurface level 0.65, and (c) Difference charge density at isosurface level 0.017 for GaN $1 \times 1 \times 3$ super unit cell.

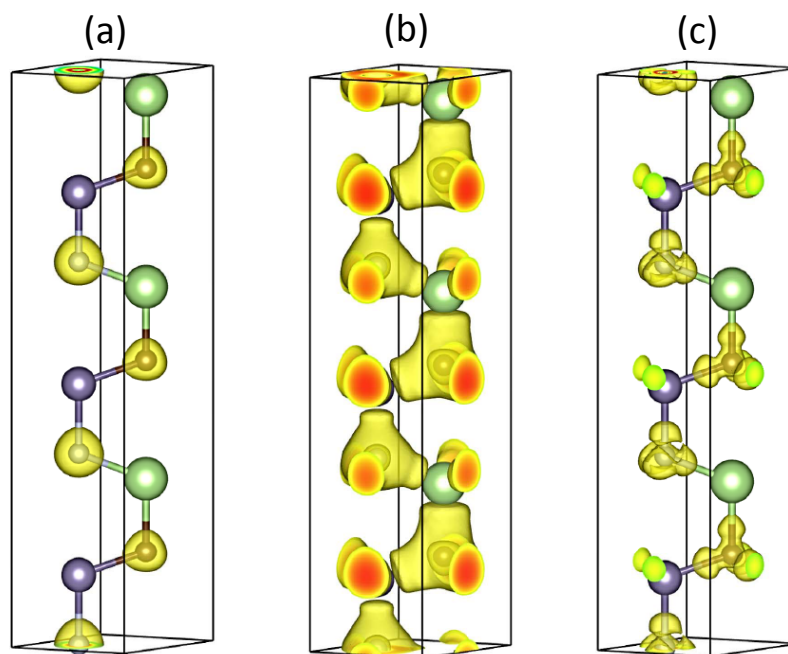


Figure S10: (Color online) (a) Charge density at isosurface level 0.17, (b) Electron localization function at isosurface level 0.65, and (c) Difference charge density at isosurface level 0.017 for S-1 $1 \times 1 \times 3$ super unit cell.

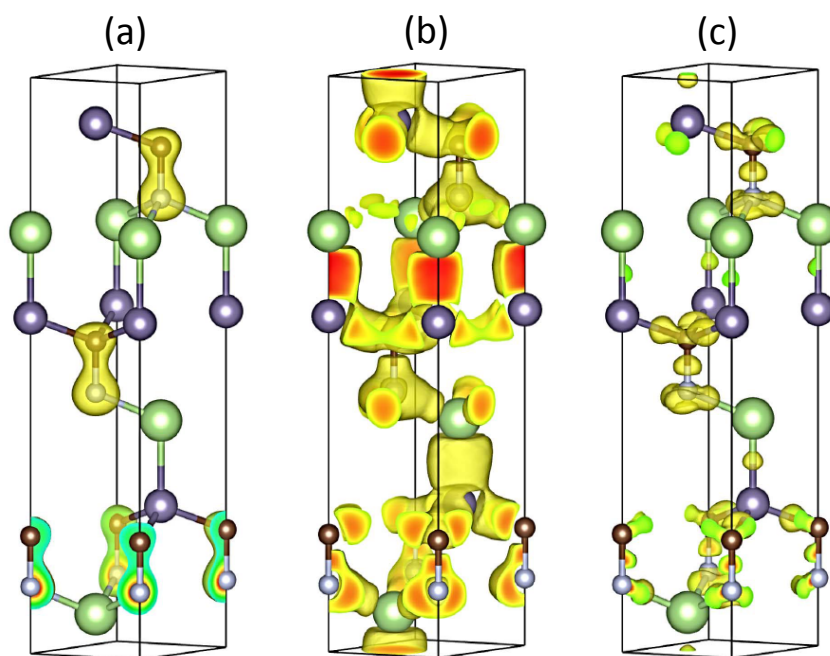


Figure S11: (Color online) (a) Charge density at isosurface level 0.17, (b) Electron localization function at isosurface level 0.65, and (c) Difference charge density at isosurface level 0.017 for S-5 $1 \times 1 \times 3$ super unit cell.

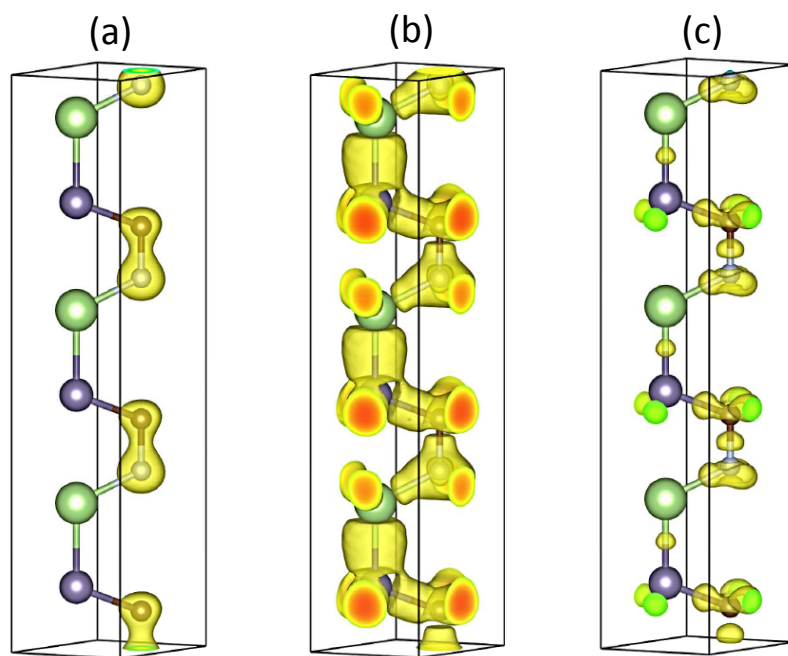


Figure S12: (Color online) (a) Charge density at isosurface level 0.17, (b) Electron localization function at isosurface level 0.65, and (c) Difference charge density at isosurface level 0.017 for S-6 $1 \times 1 \times 3$ super unit cell.

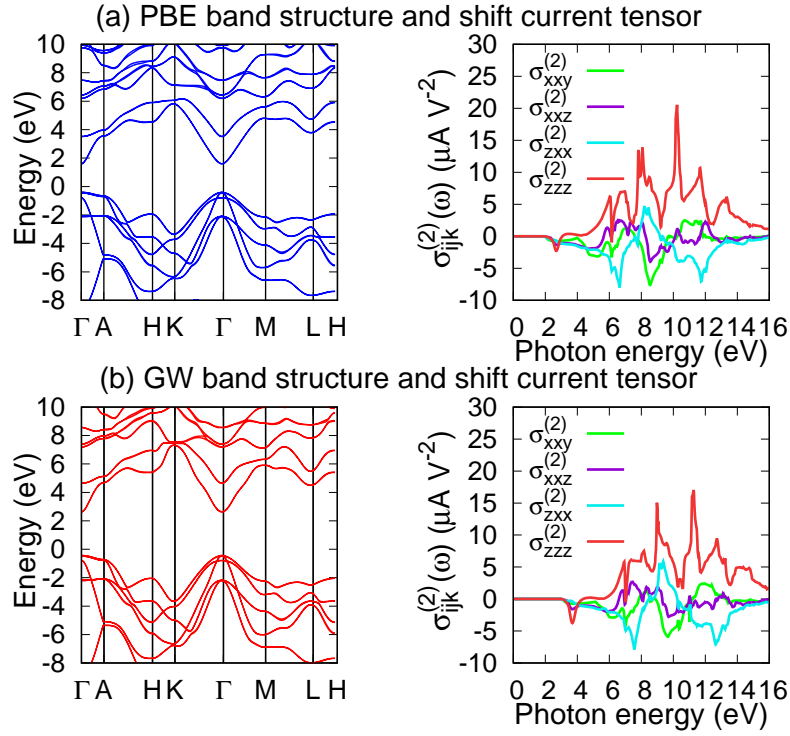


Figure S13: (Color online) Band structure and shift current conductivity tensor $\sigma_{ijk}^{(2)}(\omega)$ spectra of S-1 crystal: (a) PBE functional and (b) GW approximation performed using the Vienna Ab initio Simulation Package (VASP).

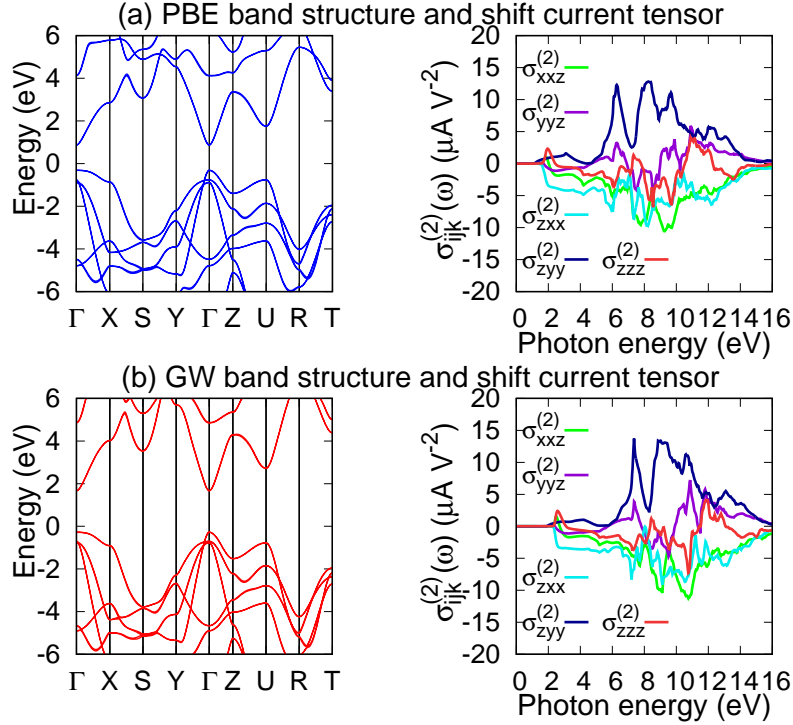


Figure S14: (Color online) Band structure and shift current conductivity tensor $\sigma_{ijk}^{(2)}(\omega)$ spectra of S-2 crystal: (a) PBE functional and (b) GW approximation performed using the Vienna Ab initio Simulation Package (VASP).

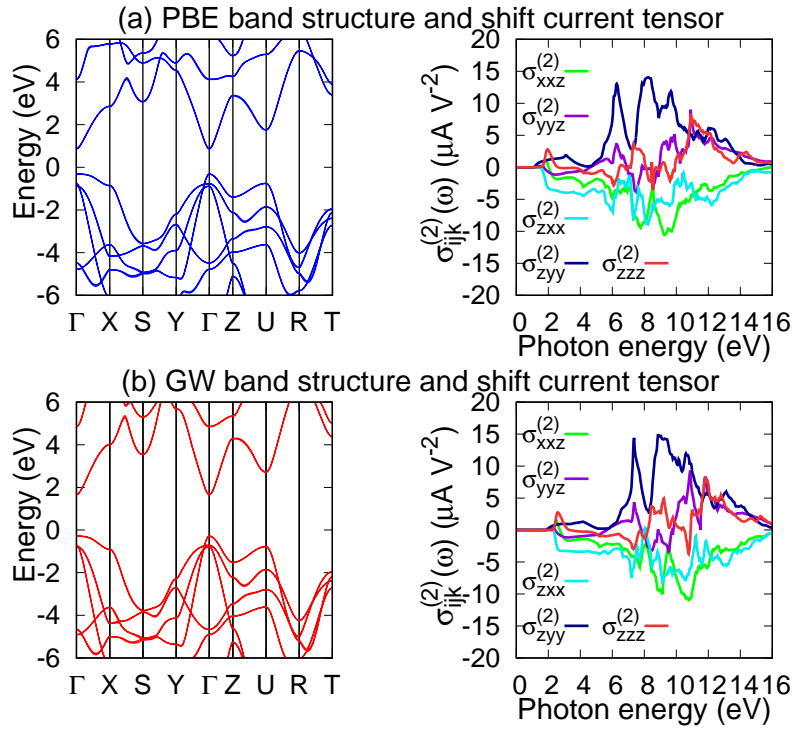


Figure S15: (Color online) Band structure and shift current conductivity tensor $\sigma_{ijk}^{(2)}(\omega)$ spectra of S-3 crystal: (a) PBE functional and (b) GW approximation performed using the Vienna Ab initio Simulation Package (VASP).

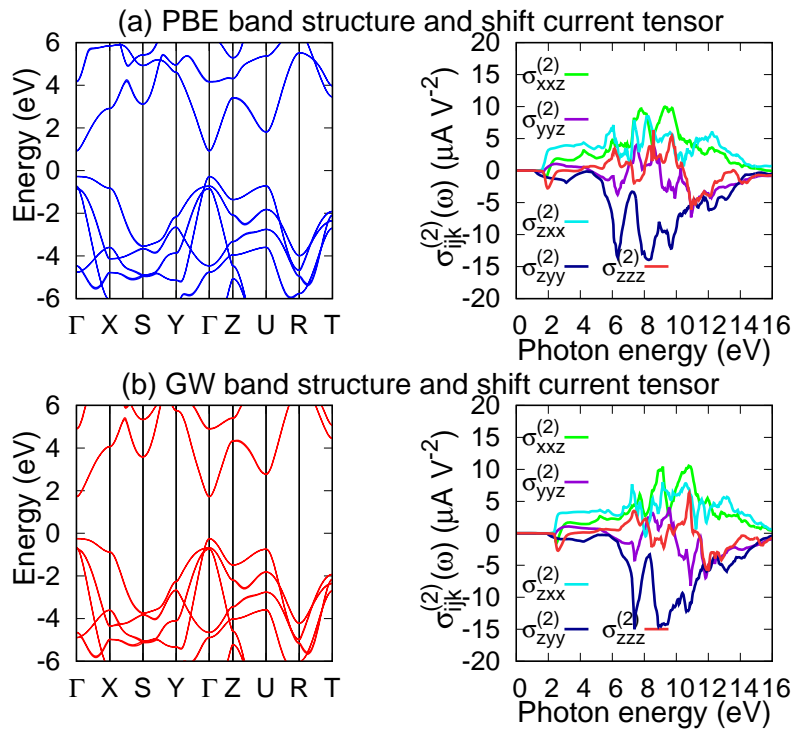


Figure S16: (Color online) Band structure and shift current conductivity tensor $\sigma_{ijk}^{(2)}(\omega)$ spectra of S-4 crystal: (a) PBE functional and (b) GW approximation performed using the Vienna Ab initio Simulation Package (VASP).

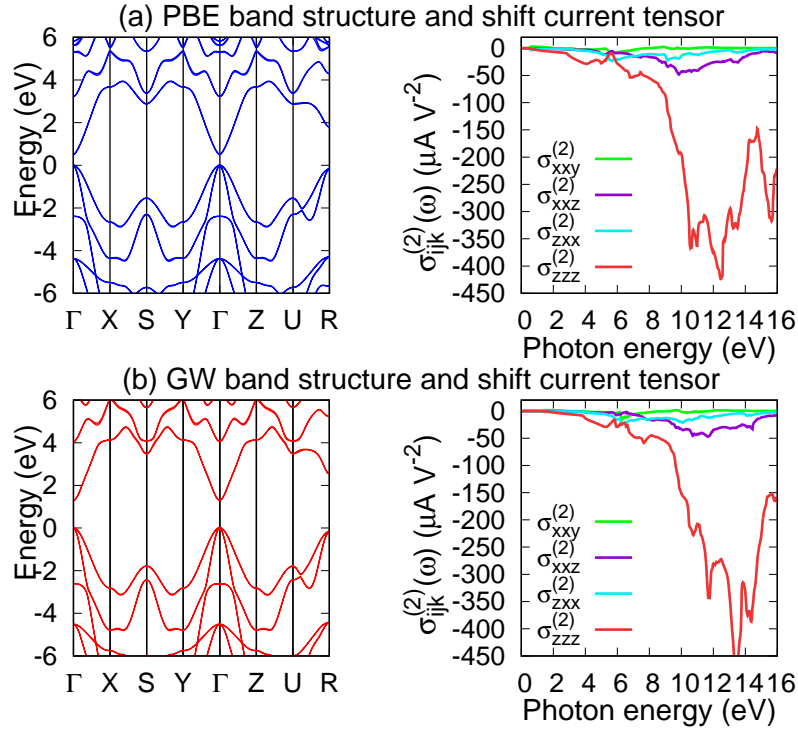


Figure S17: (Color online) Band structure and shift current conductivity tensor $\sigma_{ijk}^{(2)}(\omega)$ spectra of S-5 crystal: (a) PBE functional and (b) GW approximation performed using the Vienna Ab initio Simulation Package (VASP).

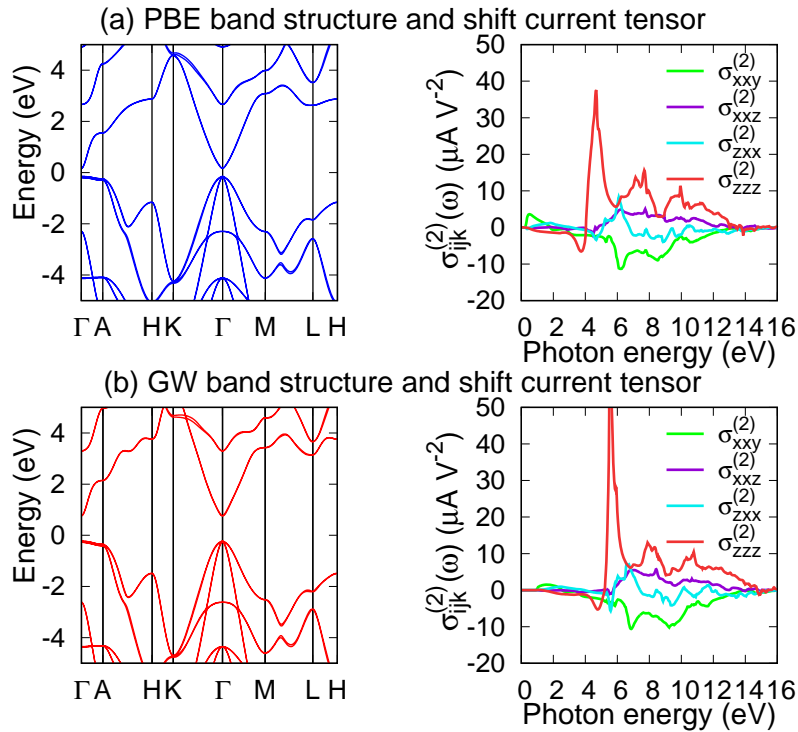


Figure S18: (Color online) Band structure and shift current conductivity tensor $\sigma_{ijk}^{(2)}(\omega)$ spectra of S-6 crystal: (a) PBE functional and (b) GW approximation performed using the Vienna Ab initio Simulation Package (VASP).

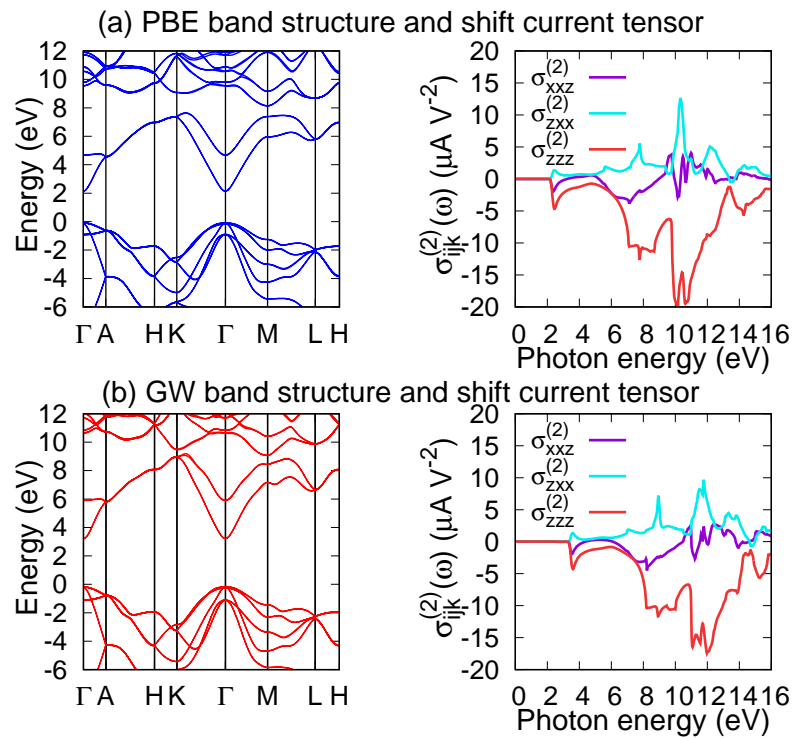


Figure S19: (Color online) Band structure and shift current conductivity tensor $\sigma_{ijk}^{(2)}(\omega)$ spectra of GaN crystal: (a) PBE functional and (b) GW approximation performed using the Vienna Ab initio Simulation Package (VASP).

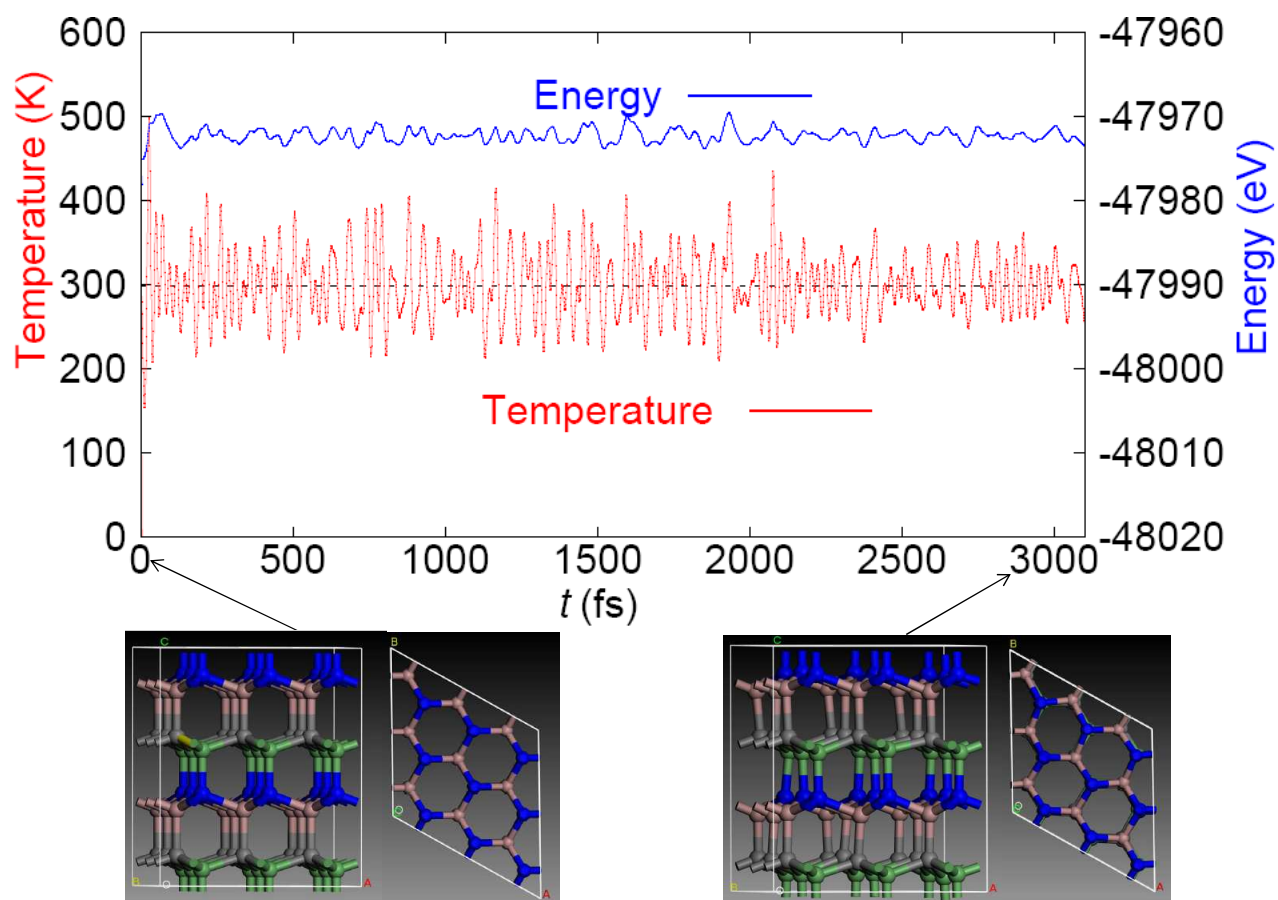


Figure S20: (Color online) S-1 crystal stacking of side and top views of geometric structures at $t=0$ and 3000 fs. Energy (blue) and temperature (red) as a function of quantum molecular dynamics (QMD) simulations time (t) at 300 K in a $3 \times 3 \times 2$ hexagonal supercell.

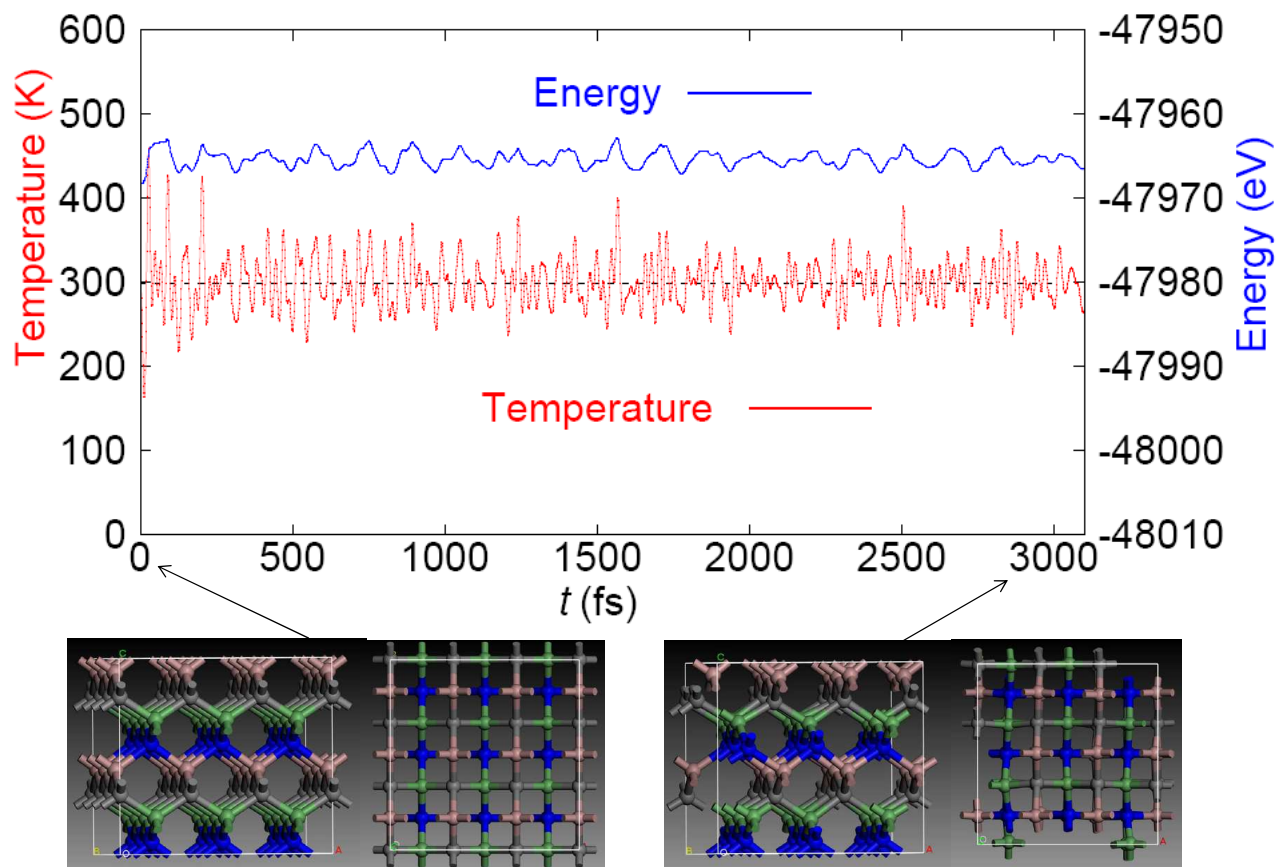


Figure S21: (Color online) S-2 crystal stacking of side and top views of geometric structures at $t=0$ and 3000 fs. Energy (blue) and temperature (red) as a function of quantum molecular dynamics (QMD) simulations time (t) at 300 K in a $3 \times 3 \times 2$ supercell.

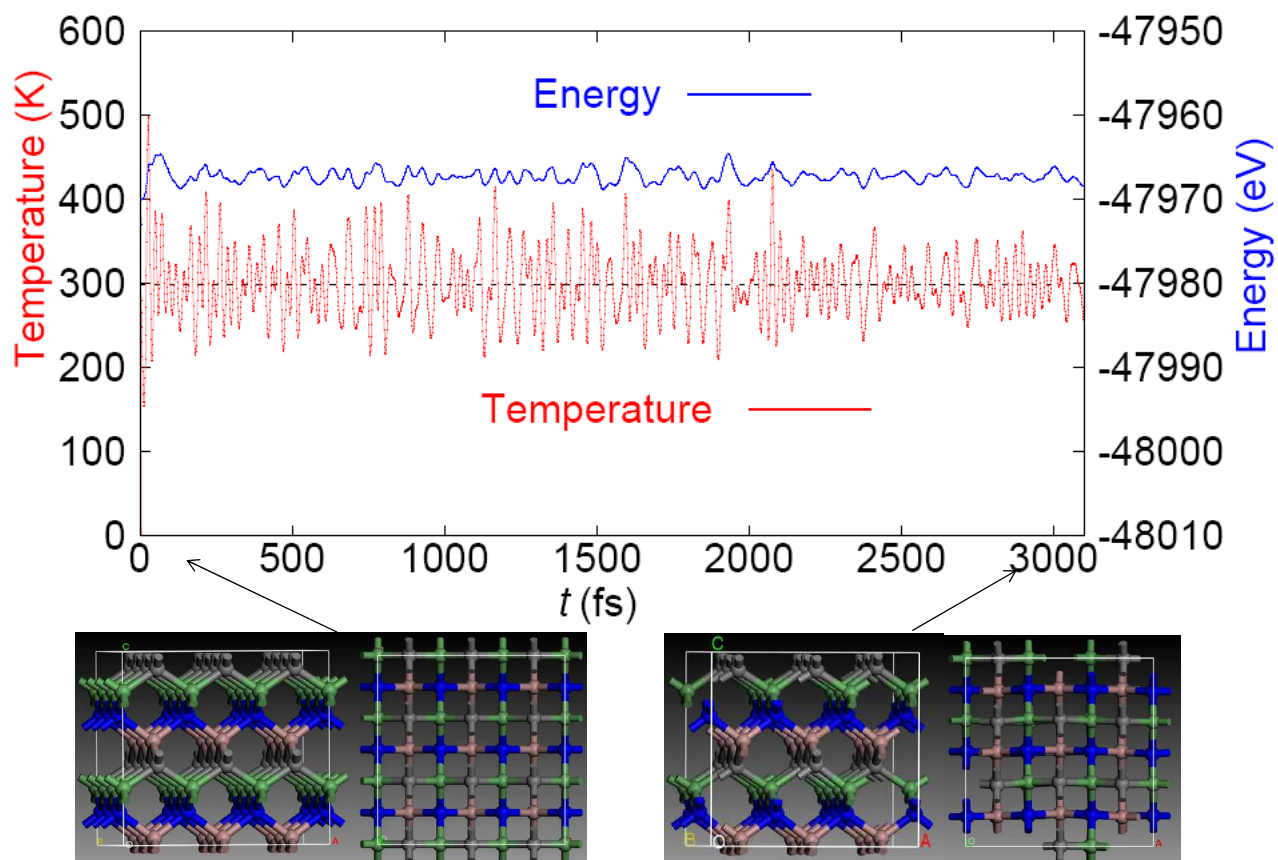


Figure S22: (Color online) S-3 crystal stacking of side and top views of geometric structures at $t=0$ and 3000 fs. Energy (blue) and temperature (red) as a function of quantum molecular dynamics (QMD) simulations time (t) at 300 K in a $3 \times 3 \times 2$ hexagonal supercell.

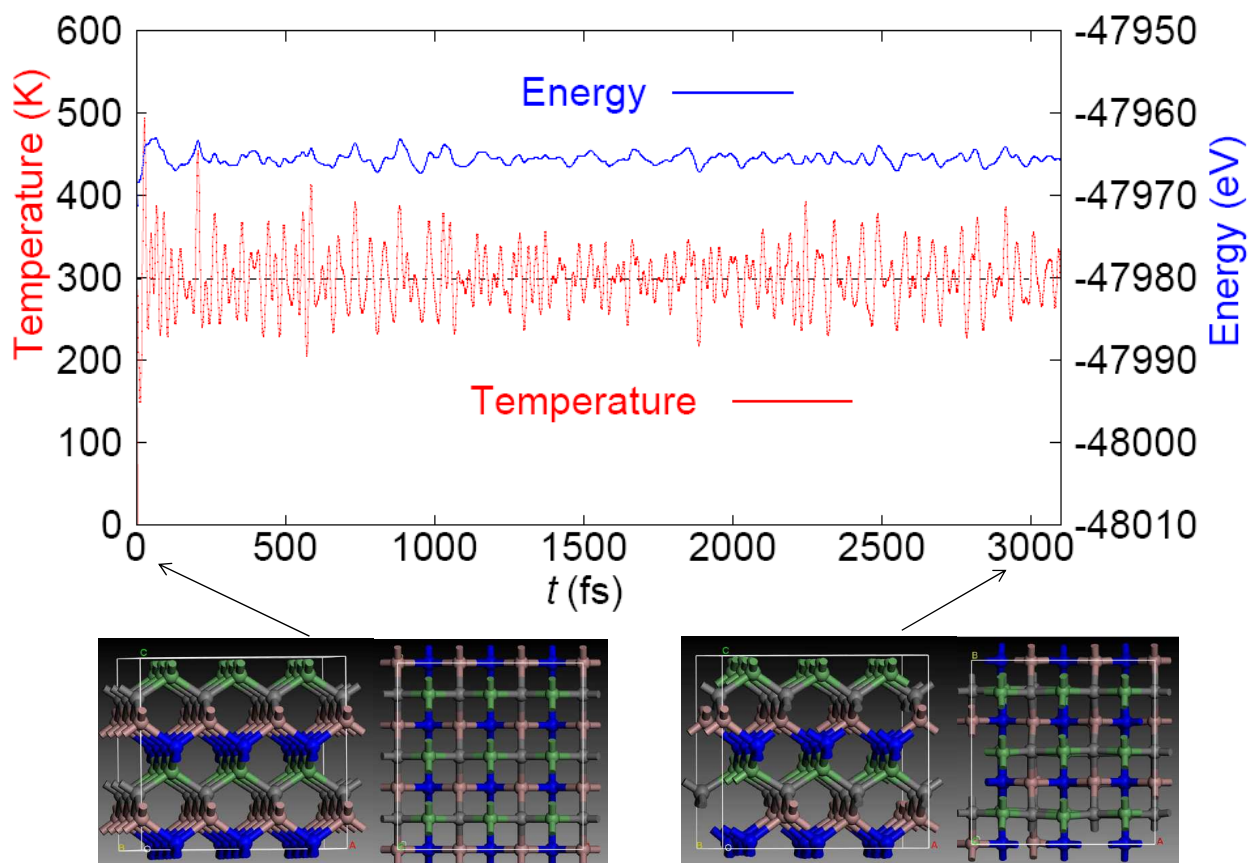


Figure S23: (Color online) S-4 crystal stacking of side and top views of geometric structures at $t=0$ and 3000 fs. Energy (blue) and temperature (red) as a function of quantum molecular dynamics (QMD) simulations time (t) at 300 K in a $3 \times 3 \times 2$ supercell.

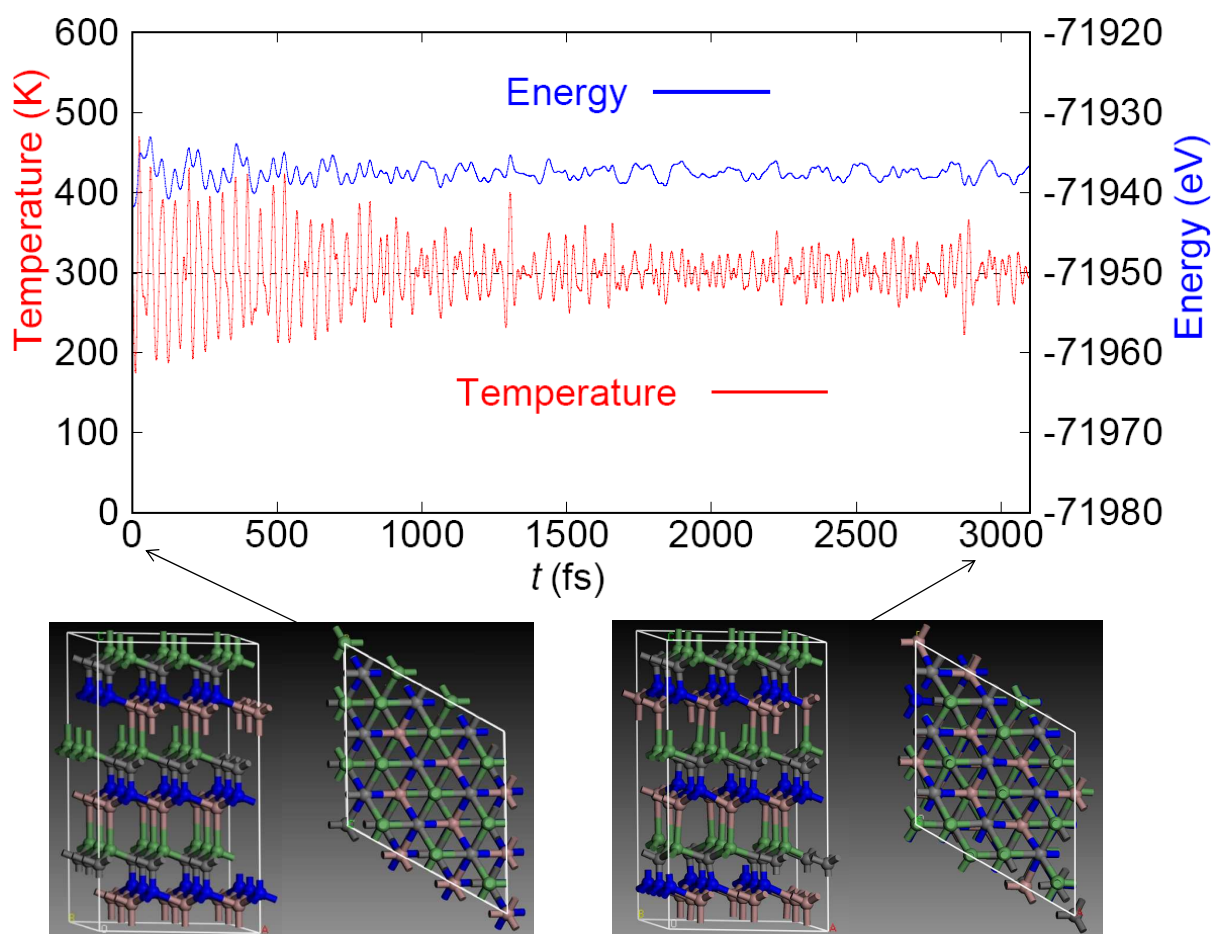


Figure S24: (Color online) S-5 crystal stacking of side and top views of geometric structures at $t=0$ and 3000 fs. Energy (blue) and temperature (red) as a function of quantum molecular dynamics (QMD) simulations time (t) at 300 K in a $3 \times 3 \times 1$ hexagonal supercell.

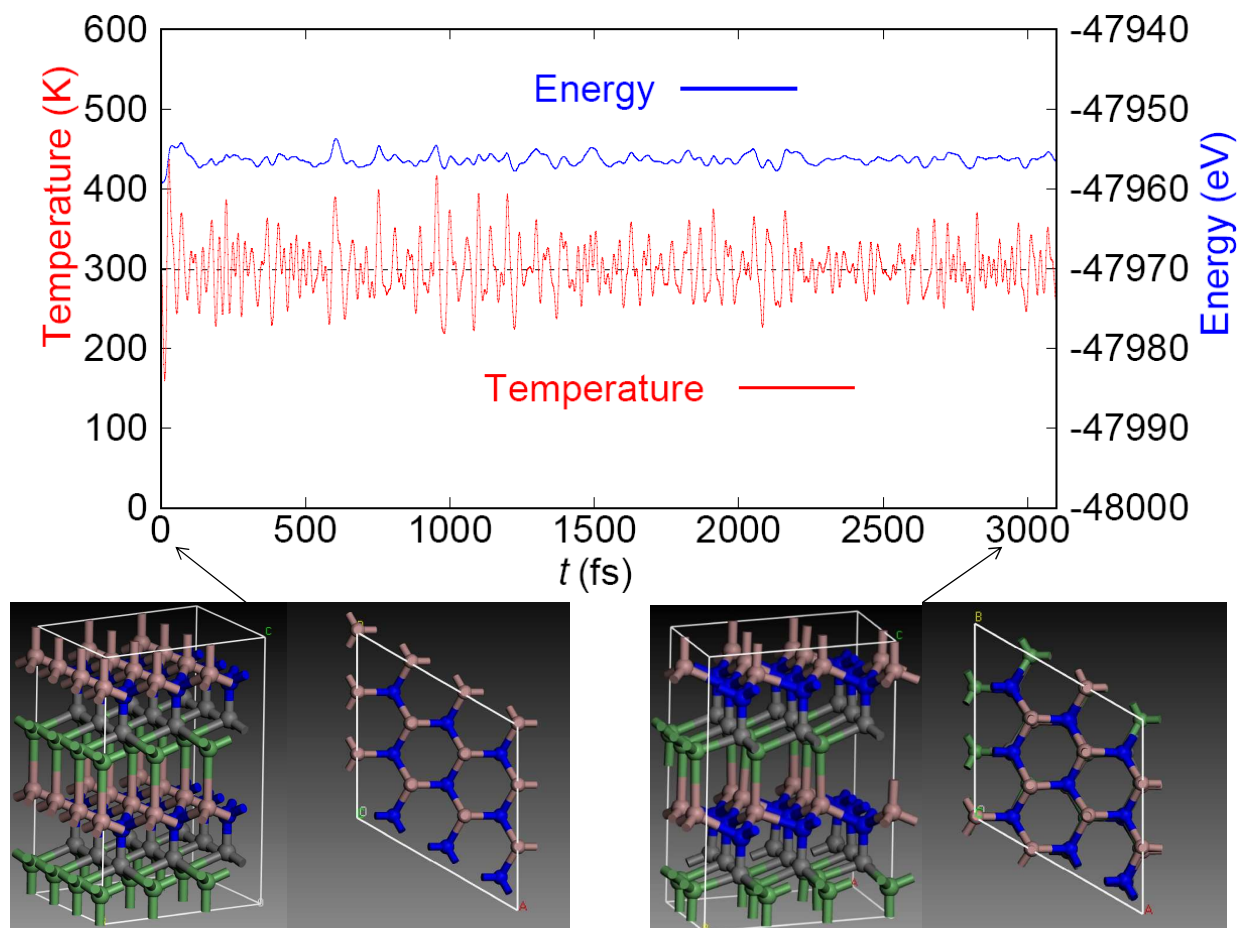


Figure S25: (Color online) S-6 crystal stacking of side and top views of geometric structures at $t=0$ and 3000 fs. Energy (blue) and temperature (red) as a function of quantum molecular dynamics (QMD) simulations time (t) at 300 K in a $3 \times 3 \times 2$ supercell.

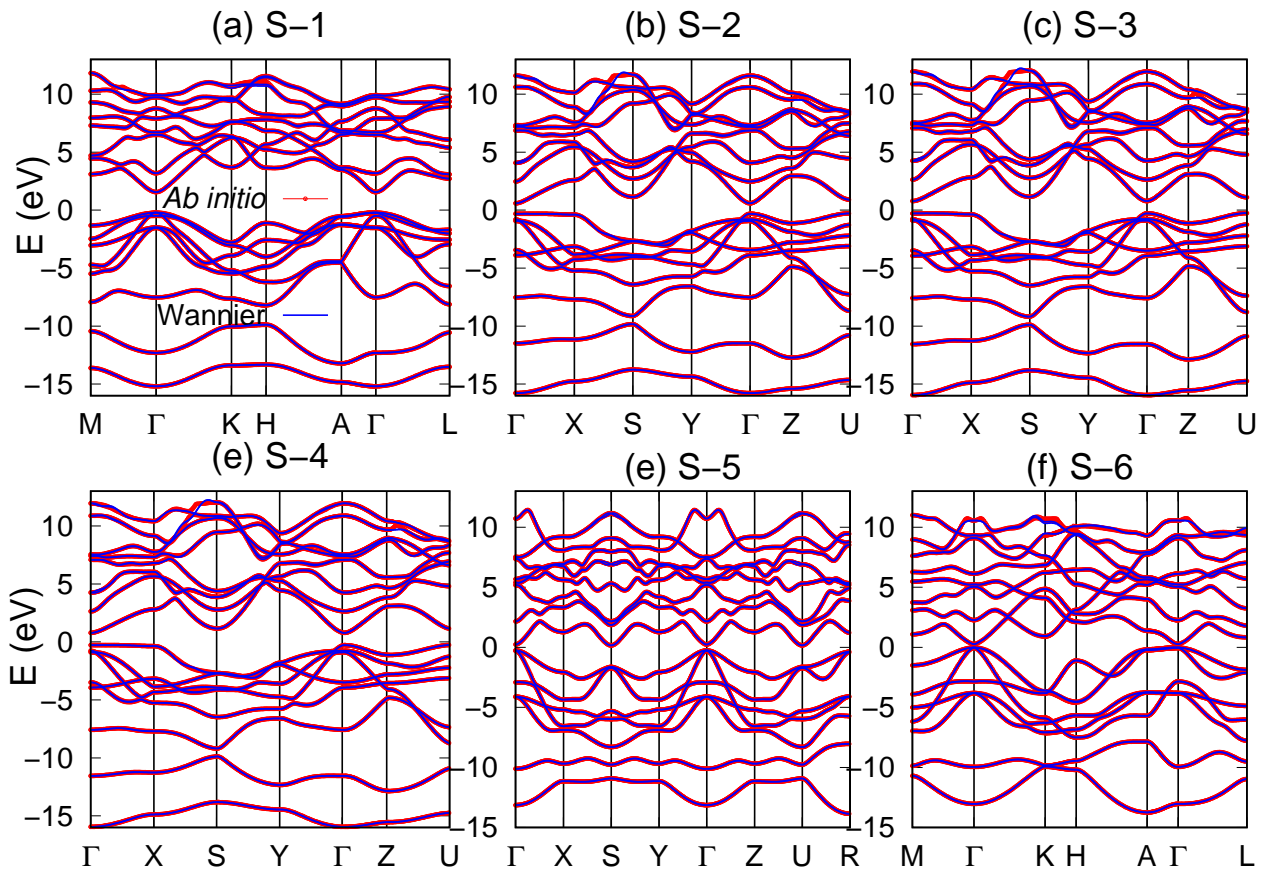


Figure S26: (Color online) The *ab initio* and Wannier-interpolated band structures of (a) S-1, (b) S-2, (c) S-3, (d) S-4, (e) S-5, and (f) S-6 crystals for the energy window.

1. Influence of Spatial Symmetry on Linear Optical Conductivity

The S-2, S-3 and S-4 belong to the C_{2v} (mm2) point group. For C_{2v} (mm2) point group, the $\hat{C}_2(z)$ and $\hat{\sigma}_v(z_y)$ symmetries play the crucial role of deciding the shape of the linear optical conductivity tensor. The $\hat{C}_2(z)$ and $\hat{\sigma}_v(z_y)$ are given as:

$$\hat{C}_2(z) = \begin{pmatrix} -1 & 0 & 0 \\ 0 & -1 & 0 \\ 0 & 0 & 1 \end{pmatrix}, \hat{\sigma}_v(z_y) = \begin{pmatrix} -1 & 0 & 0 \\ 0 & 1 & 0 \\ 0 & 0 & 1 \end{pmatrix}, \quad (\text{S1})$$

where $\hat{C}_2(z)$ displays rotational symmetry (the crystal were rotated by 90 degrees about the z axis) and $\hat{\sigma}_v(z_y)$ displays mirror reflection symmetry (a mirror plane perpendicular to x , i.e., in the $z-y$ plane). First, the $\hat{\sigma}_v(z_y)$ leads that the linear optical conductivity tensor is

$$\begin{pmatrix} \sigma_{xx} & 0 & 0 \\ 0 & \sigma_{yy} & \sigma_{yz} \\ 0 & \sigma_{zy} & \sigma_{zz} \end{pmatrix}.$$

Then, the $\hat{C}_2(z)$ further leads that the linear optical conductivity tensor should be

$$\sigma = \begin{pmatrix} \sigma_{xx} & 0 & 0 \\ 0 & \sigma_{yy} & 0 \\ 0 & 0 & \sigma_{zz} \end{pmatrix}. \quad (\text{S2})$$

The S-1, S-5 and S-6 belong to the C_{3v} (3m) point group. For C_{3v} (3m) point group, the $\hat{C}_3(z)$ and $\hat{\sigma}_v(z_y)$ symmetries play the crucial role of deciding the shape of the linear optical conductivity tensor. The $\hat{C}_3(z)$ and $\hat{\sigma}_v(z_y)$ are given as:

$$\hat{C}_3(z) = \begin{pmatrix} -\frac{1}{2} & -\frac{\sqrt{3}}{2} & 0 \\ \frac{\sqrt{3}}{2} & -\frac{1}{2} & 0 \\ 0 & 0 & 1 \end{pmatrix}, \hat{\sigma}_v(z_y) = \begin{pmatrix} -1 & 0 & 0 \\ 0 & 1 & 0 \\ 0 & 0 & 1 \end{pmatrix}, \quad (\text{S3})$$

where $\hat{C}_3(z)$ displays rotational symmetry (the crystal were rotated by 120 degrees about the z axis)

and $\hat{\sigma}_v(z,y)$ displays mirror reflection symmetry (a mirror plane perpendicular to x , i.e., in the $z-y$ plane). First, The $\hat{\sigma}_v(z,y)$ leads that the linear optical conductivity tensor is

$$\begin{pmatrix} \sigma_{xx} & 0 & 0 \\ 0 & \sigma_{yy} & \sigma_{yz} \\ 0 & \sigma_{zy} & \sigma_{zz} \end{pmatrix}.$$

Then, the $\hat{C}_3(z)$ further leads that the linear optical conductivity tensor should be

$$\sigma = \begin{pmatrix} \sigma_{xx} & 0 & 0 \\ 0 & \sigma_{xx} & 0 \\ 0 & 0 & \sigma_{zz} \end{pmatrix} \quad (S4)$$

2. Influence of Spatial Symmetry on Shift Current Conductivity

The S-2, S-3 and S-4 belong to the C_{2v} (3m) point group. For C_{2v} (mm2) point group, the $\hat{C}_2(z)$ and $\hat{\sigma}_v(z,y)$ symmetries play the crucial role of deciding the shape of the shift current conductivity tensor. First, the $\hat{\sigma}_v(z,y)$ leads that the shift current conductivity tensor should be

$$\begin{pmatrix} 0 & 0 & 0 & 0 & \sigma_{xxz}^{(2)} & \sigma_{xxy}^{(2)} \\ \sigma_{yxx}^{(2)} & \sigma_{yyy}^{(2)} & \sigma_{yzz}^{(2)} & \sigma_{yyz}^{(2)} & 0 & 0 \\ \sigma_{zxx}^{(2)} & \sigma_{zyy}^{(2)} & \sigma_{zzz}^{(2)} & \sigma_{zyz}^{(2)} & 0 & 0 \end{pmatrix}.$$

Then, the $\hat{C}_2(z)$ further leads that the shift current conductivity tensor should be

$$\begin{pmatrix} 0 & 0 & 0 & 0 & \sigma_{xxz}^{(2)} & 0 \\ 0 & 0 & 0 & \sigma_{yyz}^{(2)} & 0 & 0 \\ \sigma_{zxx}^{(2)} & \sigma_{zyy}^{(2)} & \sigma_{zzz}^{(2)} & 0 & 0 & 0 \end{pmatrix} \quad (S5)$$

The S-1, S-5 and S-6 belong to the C_{3v} (3m) point group. For C_{3v} (mm2) point group, the $\hat{C}_3(z)$ and $\hat{\sigma}_v(z,y)$ symmetries play the crucial role of deciding the shape of the shift current conductivity

tensor. First, the $\hat{\sigma}_v(z)$ leads that the shift current conductivity tensor should be

$$\begin{pmatrix} 0 & 0 & 0 & 0 & \sigma_{xxz}^{(2)} & \sigma_{xxy}^{(2)} \\ \sigma_{yxx}^{(2)} & \sigma_{yyy}^{(2)} & \sigma_{yzz}^{(2)} & \sigma_{yyz}^{(2)} & 0 & 0 \\ \sigma_{zxx}^{(2)} & \sigma_{zyy}^{(2)} & \sigma_{zzz}^{(2)} & \sigma_{zyz}^{(2)} & 0 & 0 \end{pmatrix}.$$

Then, the $\hat{C}_3(z)$ further leads that the shift current conductivity tensor should be

$$\begin{pmatrix} 0 & 0 & 0 & 0 & \sigma_{xxz}^{(2)} & \sigma_{xxy}^{(2)} \\ \sigma_{xxy}^{(2)} & -\sigma_{xxy}^{(2)} & 0 & \sigma_{xxz}^{(2)} & 0 & 0 \\ \sigma_{zxx}^{(2)} & \sigma_{zxx}^{(2)} & \sigma_{zzz}^{(2)} & 0 & 0 & 0 \end{pmatrix}. \quad (S6)$$

The GaN belongs to the point group C_{6v} ($6mm$). The $\hat{C}_6(z)$ (the crystal were rotated by 60 degrees about the z axis)) and $\hat{\sigma}_v(z)$ symmetries play the crucial role of deciding the shape of the shift current conductivity tensor, where

$$\hat{C}_6(z) = \begin{pmatrix} \frac{1}{2} & \frac{\sqrt{3}}{2} & 0 \\ -\frac{\sqrt{3}}{2} & \frac{1}{2} & 0 \\ 0 & 0 & 1 \end{pmatrix}. \quad (S7)$$

First, the $\hat{\sigma}_v(z)$ leads that the shift current conductivity tensor should be leads to the shift current conductivity tensor of the form:

$$\begin{pmatrix} 0 & 0 & 0 & 0 & \sigma_{xxz}^{(2)} & \sigma_{xxy}^{(2)} \\ \sigma_{yxx}^{(2)} & \sigma_{yyy}^{(2)} & \sigma_{yzz}^{(2)} & \sigma_{yyz}^{(2)} & 0 & 0 \\ \sigma_{zxx}^{(2)} & \sigma_{zyy}^{(2)} & \sigma_{zzz}^{(2)} & \sigma_{zyz}^{(2)} & 0 & 0 \end{pmatrix}.$$

Then, the $\hat{C}_6(z)$ further leads that the shift current conductivity tensor should be

$$\begin{pmatrix} 0 & 0 & 0 & 0 & \sigma_{xxz}^{(2)} & 0 \\ 0 & 0 & 0 & \sigma_{xxz}^{(2)} & 0 & 0 \\ \sigma_{zxx}^{(2)} & \sigma_{zxx}^{(2)} & \sigma_{zzz}^{(2)} & 0 & 0 & 0 \end{pmatrix}. \quad (S8)$$